



CO elimination processes over promoter-free hydroxyapatite supported palladium catalysts

Zouhair Boukha ^{*}, José L. Ayastuy, Juan R. González-Velasco, Miguel A. Gutiérrez-Ortiz

Chemical Technologies for Environmental Sustainability Group, Department of Chemical Engineering, Faculty of Science and Technology, University of The Basque Country UPV/EHU, P.O. Box 644, E-48080 Bilbao, Spain

ARTICLE INFO

Article history:

Received 22 June 2016

Received in revised form 5 August 2016

Accepted 16 August 2016

Available online 17 August 2016

Keywords:

Hydroxyapatite

Pd particle size

OSC

OSCC

COPROX

WGS

ABSTRACT

The catalytic performance of synthesised calcium-deficient hydroxyapatite supported Pd catalysts are examined for various CO elimination processes, namely CO total oxidation, CO preferential oxidation and water gas shift reactions. The prepared samples loaded with different amounts of palladium (0.5–2%) are thoroughly characterised by a wide number of analytical techniques including N_2 physisorption, XRD, H_2 -TPR, TEM, CO-TPD, H_2 chemisorption, OSCC and OSC techniques. The characterisation results show that, besides an incorporation of 0.3 wt% Pd into hydroxyapatite structure, on the Pd(0.5)/HAP sample, small Pd particle sizes (7.6 nm) are deposited on the HAP support surface presenting relatively high dispersion (19%). The OSCC and OSC studies show that the highly dispersed Pd species lying on the HAP surface present high reducibility and high oxygen mobility.

In the three investigated CO elimination processes the Pd(0.5)/HAP catalyst proves to be highly active and exhibits higher stability compared to that of the Pd(1)/HAP and Pd(2)/HAP catalysts. The catalytic performance of the series of the catalysts demonstrates their structure-sensitivity in the investigated processes. The latter are remarkably enhanced in the presence of small Pd particle sizes which provide high reducibility and high oxygen storage capacity. Moreover, the performances of the Pd/HAP catalysts evidence the potential of HAP support as promising alternative to those reported in the available literature.

© 2016 Elsevier B.V. All rights reserved.

1. Introduction

The use of hydrogen as fuel is a promising alternative to produce clean and efficient energy [1,2]. However, due to its production mainly via the reforming of hydrocarbons its purification is necessary to eliminate the traces of CO in the hydrogen stream; especially, when the posterior use can only tolerate very low concentration of CO (<100 ppm) as in the case of the polymer electrolyte membrane fuel cell (PEMFC) applications. For this purpose, the water gas shift reaction (WGSR) and CO preferential oxidation (COPROX) processes are applied as post-reforming stages for removing most of the CO and producing additional H_2 .

Generally, catalysts for total CO oxidation (COTOX) consist of transition metal oxides (Cu, Co and Mn) and supported noble metal (Pt, Pd, Au and Ru) catalysts [1–4]. Despite the economical consideration that motivates their use the activity of transition metals is still

relatively low compared to the promoted noble metals. Moreover, the former are sensitive to H_2O [5]. Among the noble metal catalysts, Pd-based catalysts have attracted a considerable attention during the past several decades.

Usually, the Pd active phases are supported on active (such as CeO_2 , MnO_x , TiO_2 and Fe_2O_3) or inert (such as Al_2O_3 graphene and SiO_2) metal oxides presenting relatively high specific surface area [5–14]. Liu et al. [8] studied the role of FeO_x support for oxygen supply, compared to alumina support, during CO oxidation reaction. They found that CO oxidation over Pd/ FeO_x occurs on two adjacent active sites (Pd for CO and FeO_x for oxygen) with low activation energy (34 kJ mol^{-1}), compared to that obtained on Pd/ Al_2O_3 catalyst (71 kJ mol^{-1}), which accounts for the dramatic difference in activity from Al_2O_3 and Fe_2O_3 supported Pd. Furthermore, the effect of some additives, such as ceria, cobalt, zinc and alkaline earth metals as promoters to enhance the activity of Pd catalysts, has been extensively studied [11–13]. The main objectives are the stabilization of the Pd species structures and the enhancement of the redox properties of the surface active phases which play an important role in the catalytic properties of these systems in CO oxidation.

* Corresponding author.

E-mail addresses: zouhair.boukha@ehu.eus, zouhair.boukha@hotmail.com (Z. Boukha).



Nevertheless, Pd catalysts show very low activity and selectivity in the presence of hydrogen (COPROX process) [15–17]. The oxidation of H₂ appeared to be greatly favoured at the expense of CO oxidation. Oh et al. [15] associated this low COPROX activity, over their Pd/Al₂O₃ catalysts, with the formation of PdO_x species which are very active in hydrogen oxidation. Also, Pozdnyakova et al. [16] observed a poor activity on Pd catalysts, even with reducible support (CeO₂). They claimed that, in the presence of hydrogen, formation of Pd β-hydride greatly suppressed the possibility of CO oxidation, because oxygen from both gas-phase and support sites (and also from PdO_x) reacts rapidly with H₂ to form water, which desorbs easily.

On the other hand, Pd catalysts supported on various supports were also studied in WGS reaction [18–23]. In this case, reducible supports (CeO₂, TiO₂, Fe₂O₃ and Co₂O₃) are frequently used. According to Sekine et al. [19] despite their lower initial activity the Pd/LaCoO₃ catalysts exhibit superior stability compared to Pt/LaCoO₃ catalysts. They also reported that Pd-Pt/LaCoO₃ catalyst presents higher activity and stability than that of a commercially available catalyst (Cu-ZnO). Hilaire et al. [20] showed that Pd/ceria exhibited much higher activities than either ceria alone or Pd/silica, demonstrating a cooperative effect between Pd and ceria. Moreover, they proposed a mechanism involving a redox process which consists on the oxidation of reduced ceria by water and then transferring oxygen to the active metal to react with adsorbed CO. In their study on the Pd model catalysts, Pd/Al₂O₃ and Pd/CZ, Lupescu et al. [23] concluded that to prolong the performance throughout the life of the catalyst a relatively high dispersion of Pd should be maintained. This also implies the importance of the support applied to disperse the Pd species.

To resume, the applicability of Pd catalyst is a topic of high interest both scientifically and technically. Various supports are used to disperse the Pd species and to generate new interactions which promote their activity. In the present work, we study the applicability of hydroxyapatite (HAP), Ca₁₀(PO₄)₆(OH)₂, as a porous support of the Pd species for three CO elimination processes (COTOX, COPROX and WGS). Our interest in this kind of materials is justified by the flexibility of its crystal structure and its high ion-exchange ability which may lead to the speciation of the metal active phases [24–26]. Moreover, HAP offers the possibility of tuning the surface chemical properties by varying the calcium/phosphorus ratio [24–26]. These interesting characteristics confer to HAP materials a large room for improvement in their catalytic activity and selectivity. Though a number of studies dealing with hydroxyapatite as support are presently available [24–26], to the best of our knowledge, the applications of the prepared Pd(x)/hydroxyapatite in such reactions and our approach to explain their catalytic behavior have not been yet investigated. Interesting conclusions have been drawn from the correlation between the distribution of Pd active species and their performance in the three investigated processes.

2. Experimental

2.1. Preparation of the catalysts

Calcium-deficient hydroxyapatite support (HAP), with Ca/P molar ratio equal to 1.50, was synthesized adding drop wise a boiled aqueous solution of calcium nitrate to a solution of (NH₄)₂HPO₄. The precipitate was re-dissolved in a nitric acid solution and neutralized with ammonia at pH 10. The resulting mixture was maintained under stirring at 80 °C for 16 h. After filtration, the recovered solid was washed well with purified water then dried at 120 °C and finally calcined at 500 °C for 4 h.

The Pd(x)/HAP catalysts were prepared by impregnation of the corresponding support by tetraamminepalladium (II) chloride

monohydrate where x is the Pd wt.% content (Table 1). The prepared catalysts were calcined at 500 °C (4 h). The activated samples were obtained after a reduction under 20%H₂/He at 200 °C for 2 h followed by a treatment at 500 °C in a flow of pure He.

2.2. Characterisation techniques

The volumetric N₂ adsorption at –196 °C was performed on an automatic apparatus Micromeritics, model TRISTAR II 3020 apparatus. The pre-treatments applied to the samples consisted of a cleaning, at 300 °C (overnight), under nitrogen flow. The specific areas of the samples were determined in line with the standard BET procedure, using nitrogen adsorption taken in the relative equilibrium pressure interval of 0.03–0.3.

X-ray diffraction (XRD) studies were conducted on a X'PERT-MPD X-ray diffractometer with Cu K α radiation ($\lambda = 1.5406 \text{ \AA}$) and Ni filter. The X-ray tube was operated at 40 kV and 40 mA. The samples were scanned between 10° and 100° (2 θ), and the X-ray diffraction line positions were determined with a step size of 0.01° and a counting time of 2.5 s per step. Phase identification was conducted by comparison with JCPDS database cards.

The morphology, size and dispersion of the palladium particles lying on the reduced Pd(x)/HAP surface were examined by transmission electron microscopy (TEM). The TEM studies were performed on a Philips CM200 transmission electron microscope equipped with LaB₆ filament operating at 200 kV and combined with X-ray energy dispersive spectroscopy (X-EDS) techniques. The latter was used to confirm the absence of chlorine phases from our samples surface. The average diameter of palladium particles was obtained from the measurement of at least 300 particles using ImageJ software. The corresponding values for palladium dispersion, D_{TEM}, and specific palladium surface area were calculated according to a procedure previously described by Borodzinski et al. [27].

The reducibility of the Pd(x)/HAP catalysts was examined by temperature-programmed reduction (H₂-TPR) on a Micromeritics AutoChem 2920 instrument equipped with a thermal conductivity detector (TCD). Firstly, all the samples were pre-treated in an oxygen stream (5%O₂/He, 50 cm³ min^{–1}) at 500 °C for 1 h and then cooled to –30 °C in a flow of He (50 cm³ min^{–1}). The reducing gas was 5%H₂/Ar with a flow rate of 50 cm³ min^{–1}. The temperature range explored was from –30 °C to 600 °C, with a heating rate of 10 °C min^{–1}. This temperature was maintained for 30 min. The produced water was trapped in a cold trap, and the consumption of H₂ was quantitatively measured by time integration of the H₂-TPR profiles.

The H₂ chemisorption measurements were carried out on the same experimental setup, used for H₂-TPR experiments. The catalysts (80 mg) were submitted to a pre-reduction at 200 °C (2 h) in a flow 5%H₂/Ar (50 cm³ min^{–1}) followed by a treatment with Ar (50 cm³ min^{–1}) at 500 °C. H₂ pulses (5%H₂/Ar, loop volume: 0.5 cm³) were then injected in Ar carrier (50 cm³ min^{–1}) over the sample, at 70 °C [28]. The Pd dispersion, D_{chem}, defined as the active metal fraction exposed (D_{chem} = Pd_s/Pd_{tot}) was determined on the assumption of a unity adsorption stoichiometry (H/Pd_s = 1); where “Pd_s” represents the surface Pd atoms and “Pd_{tot}” represents the total amounts of Pd. The mean diameter of Pd particles was calculated, assuming that Pd particles have a spherical shape, from the following expressions [27]:

- i) For D_{chem} in the range 0.01–0.2: d(nm) = 1.404/D_{chem} (1)
- ii) For D_{chem} in the range 0.2–0.84: d(nm) = 1.180/D_{chem} (2)

The temperature programmed desorption of CO studies (CO-TPD) were carried out on the same experimental setup, used for H₂-TPR experiments, coupled to a MKS Cirrus LM99 mass

Table 1

Chemical composition and textural properties of the Pd(x)/HAP catalysts (calcined, reduced and used in COTOX, COPROX and WGR reactions).

Catalysts	Pd, wt.%		S_{BET} , $\text{m}^2 \text{g}^{-1}$	Pore volume, $\text{cm}^3 \text{g}^{-1}$	Pore size, nm
HAP	0.00 (1.50)	Calcined	52.0	0.45	30.3
Pd(0.5)/HAP	0.56 (1.51)	Calcined	48.0	0.39	28.0
		Reduced	44.0	0.37	31.3
		COTOX	45.0	0.39	28.7
		COPROX	29.0	0.32	28.3
		WGS	46.0	0.39	28.3
Pd(1)/HAP	0.99 (1.52)	Calcined	48.0	0.40	30.0
		Reduced	44.0	0.38	30.8
		COTOX	43.0	0.32	27.8
		COPROX	30.0	0.32	30.4
		WGS	46.0	0.41	29.4
Pd(2)/HAP	2.05 (1.53)	Calcined	48.0	0.37	29.0
		Reduced	42.0	0.35	30.5
		COTOX	44.0	0.35	26.6
		COPROX	27.0	0.30	27.0
		WGS	44.0	0.39	28.6

Values in brackets correspond to $(\text{Ca} + \text{Pd})/\text{P}$ molar ratios.

spectrometer. The catalysts were submitted to a pre-treatment consisting on their reduction at 200°C (2 h) in a flow $5\% \text{H}_2/\text{Ar}$ ($50 \text{ cm}^3 \text{ min}^{-1}$) followed by a treatment with He ($50 \text{ cm}^3 \text{ min}^{-1}$) at 500°C . The adsorption of CO was performed at -120°C in a flow of $5\% \text{CO}/\text{He}$ ($50 \text{ cm}^3 \text{ min}^{-1}$) for 1 h. After CO adsorption the samples were treated with He for 1 h and heated at $10^\circ\text{C min}^{-1}$ up to 500°C in flowing He ($50 \text{ cm}^3 \text{ min}^{-1}$). The MS signals ($m/z = 28, 44$ and 18) assigned to CO, CO_2 and H_2O , respectively, were followed. Note that the quantification of CO amount was corrected taking into account the contribution of the signal $m/z:44$.

The Oxygen Storage Complete Capacity (OSCC) and Oxygen Storage Capacity (OSC) experiments at different temperatures (150°C , 200°C , 250°C , 300°C , 350°C and 400°C) were carried out on the same experimental setup coupled to MKS Cirrus LM99 mass spectrometer. The catalysts (25 mg, $40\text{--}80 \mu\text{m}$) were submitted to a reduction at 200°C (2 h) in a flow $5\% \text{H}_2/\text{Ar}$ followed by a treatment with He at 500°C . For the OSCC measurements, the samples were submitted to ten O_2 pulses ($5\% \text{O}_2/\text{He}$, loop volume: 5 cm^3), injected in He carrier, followed by ten CO pulses ($5\% \text{CO}/\text{He}$, loop volume: 5 cm^3). The OSCC values were determined from the sum of the CO_2 amounts formed after each CO pulse. After degas in a He flow OSC measurements were performed on the same samples. The latter were submitted to six alternating series of pulses ($\text{CO}-\text{O}_2$) where the OSC was determined as the average amount of the formed CO_2 for each CO pulse.

2.3. Catalytic tests

The catalytic tests were performed, with flow/mass ratio of $1333 \text{ cm}^3 \text{ min}^{-1} \text{ g}^{-1}$, in a tubular flow reactor operating at atmospheric pressure using 150 mg of the catalyst. Prior to running the catalytic experiments, the catalysts were submitted to a pre-treatment routine consisting on their reduction at 200°C (2 h) in a flow $20\% \text{H}_2/\text{He}$ followed by a treatment with He at 400°C . Three different feed gas mixtures with the same oxygen excess ($\lambda = 2$) ($\text{P}_{\text{O}_2}/\text{P}_{\text{CO}} = 2$) and balanced with He, to reach a total flow rate of $200 \text{ cm}^3 \text{ min}^{-1}$, were used in each reaction as follows:

- 1% CO and 1% O_2 in COTOX reaction.
- 1% CO, 1% O_2 and 60% H₂ in COPROX reaction.
- 1% CO and 2% H_2O in WGS reaction.

The reaction products were continuously analysed by Gas Chromatograph (Agilent Technologies 490 Micro GC) equipped with a TCD detector. Carbon monoxide conversions (X_{CO}) and selectivity to CO_2 (S_{CO_2}) were calculated by using the inlet (F^{in}) and outlet

(F^{out}) molar flow values of the two reactants (Eqs. (3) and (4), respectively):

$$X_{\text{CO}}(\%) = 100 \cdot \frac{F_{\text{CO}}^{\text{in}} - F_{\text{CO}}^{\text{out}}}{F_{\text{CO}}^{\text{in}}} \quad (3)$$

$$S_{\text{CO}_2}(\%) = 100 \cdot 0.5 \cdot \frac{F_{\text{CO}_2}^{\text{in}} - F_{\text{CO}_2}^{\text{out}}}{F_{\text{O}_2}^{\text{in}} - F_{\text{O}_2}^{\text{out}}} \quad (4)$$

Turnover frequency (TOF) values were calculated as the activity data per mole of active surface palladium determined by H_2 chemisorption experiments [2,3]. In order to assure differential reactor conditions the temperatures used for the calculations of turnover frequency (TOF) for the three tested reactions over the Pd(x)/HAP catalysts corresponded to low CO conversions (<20%). The absence of heat and mass transfer limitations were checked following the criterions described elsewhere [29].

3. Results and discussion

3.1. Characterization of the samples

3.1.1. N_2 -physorption (BET measurements)

The textural properties of the Pd(x)/HAP catalysts were examined by nitrogen adsorption-desorption measurements. The experimental N_2 physisorption isotherms for the Pd(x)/HAP catalysts in their calcined and reduced forms (not shown) show that they are characteristic of mesoporous materials exhibiting IV-type according to the IUPAC classification. The specific surface area, pore volume and average pore size are shown in Table 1. Fig. 1S (Supporting information) shows the pore size distributions for all the reduced catalysts. The pore size distribution corresponding to HAP support and the Pd(x)/HAP catalysts show a broad unimodal distribution centred at approximately 32 nm (Fig. 1S). This distribution does not change with the introduction of palladium. However, the addition of palladium (0.5–2%) to HAP produces a slight drop in its specific surface area (up to 19%) and pore volume. For instance, the specific surface area of the resultant catalysts significantly decreases from $52 \text{ m}^2 \text{ g}^{-1}$ for the HAP bare support to $48 \text{ m}^2 \text{ g}^{-1}$ for the oxidised and $42\text{--}44 \text{ m}^2 \text{ g}^{-1}$ for the reduced Pd(x)/HAP catalysts. Table 1 also lists the textural data of the used catalysts in the COTOX, COPROX and WGS reactions which will be commented below.

3.1.2. X-ray diffraction (XRD)

The Pd(x)/HAP samples were also characterised by means of X-ray powder diffraction in order to investigate the effect of the

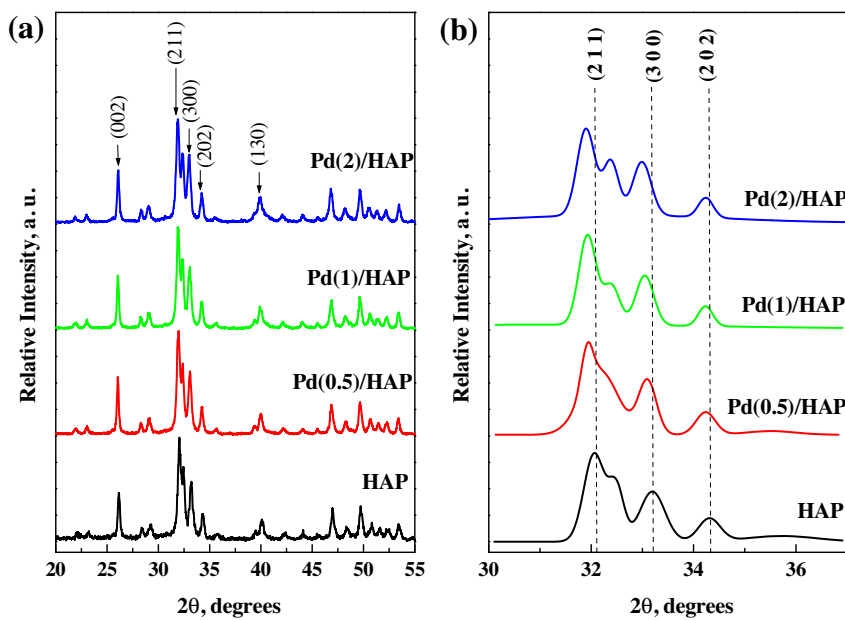


Fig. 1. (a) XRD patterns of the reduced $\text{Pd}(x)/\text{HAP}$ catalysts and (b) their magnification in the 2θ angles range of 30° – 37° .

Pd addition on their structural properties. Fig. 1a displays the XR-diffractograms corresponding to the reduced $\text{Pd}(x)/\text{HAP}$ and HAP bare support samples. The patterns of the latter are characterised by the presence of the maxima at $2\theta = 26.15^\circ, 32.06^\circ, 32.49^\circ, 33.19^\circ$ and 34.32° , among others. As expected, these 2θ angles values are slightly higher than those corresponding to stoichiometric hydroxyapatite used as reference (JCPDS 01-082-2956). This is because of the synthesised support consists of a calcium-deficient hydroxyapatite with Ca/P molar ratio equal to 1.50 (Table 1); lower than the 1.67 expected for a stoichiometric hydroxyapatite ($\text{Ca}_{10}(\text{PO}_4)_6(\text{OH})_2$). In our previous study we explained this non-stoichiometry by a loss of Ca^{2+} ions, which is corrected by insertion of H^+ ions at the expense of hydroxyl groups to ensure electroneutrality [24]. Hence, the general formula of these calcium deficient hydroxyapatite can be denoted as $\text{Ca}_{10-z}(\text{HPO}_4)_z(\text{PO}_4)_{6-z}(\text{OH})_{2-z}$ where $0 < z \leq 1$.

On the other hand, it is difficult to evidence the presence of the Pd structure peaks on the diffractograms of $\text{Pd}(x)/\text{HAP}$ catalysts; especially, the diffraction peaks corresponding to (111), (200), (220) and (311) planes which characterise the presence of metallic palladium structure. This is may be due to the overlapping of the Pd peaks with those of hydroxyapatite structure. Indeed, a comparison between the $\text{Pd}(x)/\text{HAP}$ samples shows that the peak at 40° is broader on the $\text{Pd}(1)/\text{HAP}$ and $\text{Pd}(2)/\text{HAP}$ diffractograms compared to that of $\text{Pd}(0.5)/\text{HAP}$ and HAP support, suggesting an apparent overlapping of the peak corresponding to metallic Pd (111) with that associated to hydroxyapatite (130).

Interestingly, the XRD patterns of the $\text{Pd}(x)/\text{HAP}$ catalysts show a significant evolution of the hydroxyapatite diffraction peaks which shift to lower angles with Pd loading increasing. For instance, 2θ angle corresponding to (211) reticular plane shifts from 32.06° for the HAP sample to 31.93° and 31.89° for $\text{Pd}(1)/\text{HAP}$ and $\text{Pd}(2)/\text{HAP}$ samples, respectively (Fig. 1b). These observations suggest that the presence of palladium induces a modification of the cell parameters of the HAP structure. Table 2 lists the most important structure parameters in terms of the lattice parameters, "a" and "c", and unit cell volume (V). Values corresponding to stoichiometric HAP (Ca/P:1.67) are also included for comparison. The reported data show that the lattice parameter "a" increases with increasing the Pd content. Likewise, the lattice parameter "c" calculated in all

the Pd catalysts is higher than that of the HAP bare support. This increase in "a" and "c" values with palladium addition induces an apparent increase in the unit cell volume suggesting a progressive incorporation of Pd in the HAP crystal lattice. As the ionic radius of the Pd^{2+} (100 pm) is smaller than that of Ca^{2+} (114 pm) the observed expansion might be due to an incorporation of Pd^{2+} into the cationic vacant sites rather than an ion-exchange process with Ca^{2+} sites.

3.1.3. Transmission electron microscopy (TEM)

Hydroxyapatite-supported palladium samples, reduced at 200°C , are investigated by TEM techniques. Fig. 2 shows their corresponding TEM micrographs and particle size distribution diagrams. Examination of the $\text{Pd}(0.5)/\text{HAP}$ catalyst reveals the presence of quasi-spherical Pd particles which are homogeneously dispersed on the support surface. Furthermore, the size distribution trace of these Pd particles consists of a narrow unimodal distribution with an average size of 7.6 nm corresponding to dispersion value of 19% (Table 2). This Pd dispersion value (19%) is consistent with those found by Guadet et al. [30] in their $\text{Pd}/\text{Al}_2\text{O}_3$ and $\text{Pd}/\text{La-Al}_2\text{O}_3$ systems (17–25%) presenting similar surface density of the Pd (1.2 – $1.6 \mu\text{mol m}^{-2}$). At high Pd loading the particle sizes consist of a broader distribution with an average size of 13.1 nm for $\text{Pd}(1)/\text{HAP}$ and 16.3 nm for $\text{Pd}(2)/\text{HAP}$, with relatively lower dispersion (10.4% and 8.4%, respectively) compared to the catalyst with the lowest Pd loading ($\text{Pd}(0.5)/\text{HAP}$).

On the other hand, the X-EDS analyses of the $\text{Pd}(x)/\text{HAP}$ samples after their calcination at 500°C followed by reduction at 200°C confirm the absence of Cl species on the $\text{Pd}(x)/\text{HAP}$ surface.

3.1.4. H_2 -TPR and H_2 chemisorption studies

The H_2 -TPR experiments were performed in order to determine the different Pd reducible species present in the prepared $\text{Pd}(x)/\text{HAP}$ catalysts (Fig. 3). The H_2 -TPR profiles included in Fig. 3 show typical spectra for oxidised Pd species consisting of a reduction peak at 22°C associated with the reduction of Pd oxides (Peak I) and a second negative peak at 68°C corresponding to palladium hydride (Pd-H) decomposition leading to hydrogen release (Peak II). Generally, the latter could be formed at lower temperatures equivalent to those corresponding to oxidised Pd species reduction [31–33]. Table 3 reports quantitative data corresponding to the integration of the two resulting peaks and the corresponding

Table 2

XRD and TEM data for the reduced Pd(x)/HAP catalysts.

Catalysts	XRD			TEM		
	($a \pm 0.01$), Å	($c \pm 0.002$), Å	$V, \text{Å}^3$	$D_{\text{TEM}}, \%$	d, nm	$S_{\text{Pd}}, \text{m}^2/\text{g}_{\text{cat}}$
HAP	9.3414	6.8198	515.4	–	–	–
HAP (1.67) ^a	9.4154	6.8792	528.1	–	–	–
Pd(0.5)/HAP	9.3713	6.8438	520.5	19.0	7.6	0.45
Pd(1)/HAP	9.3802	6.8418	521.3	10.4	13.1	0.49
Pd(2)/HAP	9.3941	6.8319	522.1	8.4	16.3	0.79

^a Values extracted from "JCPDS 01-082-2956" reference card.**Table 3** H_2 -TPR H_2 chemisorptions and CO-TPD data for the Pd(x)/HAP catalysts.

H ₂ -TPR						H ₂ chemisorption			CO-TPD	
Catalysts	Peak I ^a $\mu\text{mol g}^{-1}$	Peak II ^b $\mu\text{mol g}^{-1}$	$H_2(\text{I})/\text{Pd}$	$H_2(\text{II})/\text{Pd}$	$H_2^{(\text{R})}/\text{Pd}^c$	$D_{\text{chem}}, \%$	d, nm	$S_{\text{Pd}}, \text{m}^2/\text{g}_{\text{cat}}$	CO, $\mu\text{mol g}^{-1}$	$\text{CO}_2, \mu\text{mol g}^{-1}$
Pd(0.5)/HAP	23.3	3.4	0.5	0.07	0.43	21.3	5.6	0.46	182	4.0
Pd(1)/HAP	77.0	10.2	0.8	0.11	0.69	9.2	15.3	0.42	215	2.7
Pd(2)/HAP	182.0	29.0	1.0	0.15	0.85	5.0	28.1	0.44	230	2.9

^a Total amounts of H_2 consumed at 22 °C.^b Amounts of released H_2 at 68 °C.^c Data corresponding to actual amounts of consumed H_2 for the reduction process ($H_2^{(\text{R})}/\text{Pd} = H_2(\text{I})/\text{Pd} - H_2(\text{II})/\text{Pd}$).

$H_2(\text{I})/\text{Pd}$ and $H_2(\text{II})/\text{Pd}$ molar ratios determined as mole of consumed and released H_2 per mole of total palladium, respectively. Moreover, taking into account the formation of Pd hydride concurrently with the reduction of oxidised species of Pd the actual amounts of consumed H_2 for the reduction process ($H_2^{(\text{R})}/\text{Pd}$) is determined as the difference between the amounts of the consumed and the released H_2 ($H_2^{(\text{R})}/\text{Pd} = H_2(\text{I})/\text{Pd} - H_2(\text{II})/\text{Pd}$). For the Pd(0.5)/HAP sample, the calculated $H_2^{(\text{R})}/\text{Pd}$ molar ratio is around 0.43 which is lower than that expected for the reduction of stoichiometric palladium oxide (PdO). This result suggests a presence of a fraction of Pd species which does not reduce in the TPR operating conditions (heating in H_2/Ar at temperatures up to 600 °C). Similar conclusions can be extracted for the Pd(1)/HAP and Pd(2)/HAP samples which also present low $H_2^{(\text{R})}/\text{Pd}$ ratios (0.69 and 0.85, respectively). Interestingly, for all the Pd(x)/HAP samples, an estimation of this Pd non-reducible fraction show that it is around 0.29–0.31 wt% of the total weight of the sample. This is a remarkable observation indicating that it represents an upper limit for a certain interaction of Pd species with the HAP support which makes them non-reducible (up to 600 °C). In agreement with the XRD results, which proposed a possible incorporation of Pd into the hydroxyapatite network, we can conclude that the level of such incorporation is limited to 0.3 wt% Pd.

Table 3 also lists the Pd dispersion, active Pd surface area and average particle size for the Pd(x)/HAP catalysts as determined from the H_2 chemisorption measurements. Interestingly, the three catalysts exhibit comparable active Pd surface area which is around 0.42–0.47 $\text{m}_{\text{Pd}}^2 \text{g}^{-1}$ (Table 3). The comparison of the obtained results with those obtained by TEM techniques shows slight differences in the case of the Pd(0.5)/HAP and Pd(1)/HAP catalysts. By contrast, on the Pd(2)/HAP catalyst the Pd dispersion value measured by H_2 chemisorption results significantly lower (5%) compared to that determined by TEM techniques (8.4%). These observations suggested that, on the Pd-rich catalyst a large fraction of Pd is not accessible to the gas phase.

On the other hand, in agreement with a number of earlier studies from the literature the formation of palladium hydride depends on the palladium particle sizes [31–34]. In this sense, it was reported that large Pd particles easily form Pd hydride whereas small Pd particles partially inhibit its formation. According to the determined amounts of released H_2 reported in Table 3 it can be concluded that small Pd particles are deposited on the Pd(0.5)/HAP sample compared to those deposited on the higher Pd loadings samples

(1% and 2%). On the latter, the $H_2(\text{II})/\text{Pd}$ ratio corresponding to the integration of the negative peak at 68 °C reach relatively higher values (0.11–0.15) which indicate an initiation of the tridimensional growth of Pd particles. In this sense, Fig. 4 shows a clear correlation between the amounts of released H_2 during the H_2 -TPR experiments (at 68 °C) and the Pd particle sizes determined by TEM (Fig. 4a) and/or those determined by H_2 chemisorptions (Fig. 4b).

3.1.5. CO-TPD study

The thermal stability of pre-adsorbed CO on the Pd(x)/HAP catalysts was investigated by means of CO-TPD techniques. The TPD profiles of pre-adsorbed CO at –120 °C on the reduced Pd(x)/HAP catalysts are presented in Fig. 5. Data corresponding to the HAP bare support are also included for comparison. Generally, at low temperatures (<100 °C) the CO desorption peaks are associated with linearly bonded CO (weakly adsorbed CO species) while the desorption peaks centred at high temperatures (>200 °C) are attributed to bridge-bonded CO (strongly adsorbed CO species) [35].

For all the analysed samples large amounts of CO are desorbed at low temperatures which are related to linearly bonded CO (Fig. 5a). As reported in Table 3 the amount of desorbed CO from the HAP, 397 $\mu\text{mol g}^{-1}$, is much higher than those determined for the three Pd catalysts (182–230 $\mu\text{mol g}^{-1}$). It can also be observed that the amount of the weakly adsorbed CO increases with the Pd loadings increase, 182 $\mu\text{mol g}^{-1}$ for Pd(0.5)/HAP, 215 $\mu\text{mol g}^{-1}$ for Pd(1)/HAP and 230 $\mu\text{mol g}^{-1}$ for Pd(2)/HAP. This trend suggests that the high dispersion of Pd tends to decrease the density of the weak-strength adsorption sites of CO. However, the Pd(0.5)/HAP sample exclusively exhibits additional CO desorption peak which occurs at temperature around 290 °C (Fig. 5a). This fraction, that represents 4% of the total amount of desorbed CO, can be associated to the highly dispersed Pd species.

Fig. 5b displays the profiles of the formation/release of CO_2 during the CO-TPD experiments. It should be noted that in addition to CO_2 formation small amount of H_2O is observed in the desorbing gas (not shown), suggesting the occurrence of the water gas shift reaction of the adsorbed CO with the surface hydroxyl groups of the support [35–37]. On the HAP bare support the release of CO_2 starts around 180 °C which forms a broad desorption peak presenting a maximum at 350 °C (Fig. 5b). By contrast, on the Pd(x)/HAP catalysts the formation of CO_2 starts at relatively lower temperatures (around 100 °C). Likewise, the position of the CO_2 peaks seems to shift toward low temperatures compared with that of

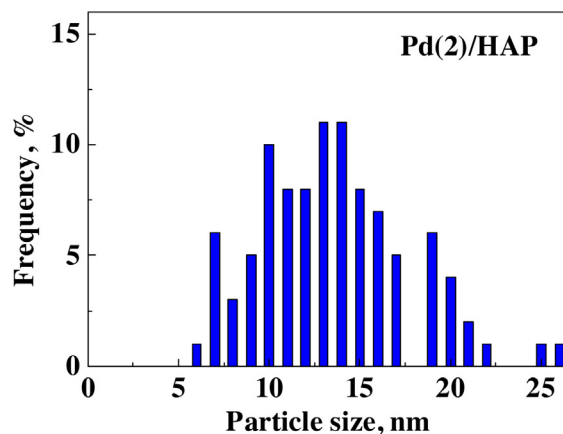
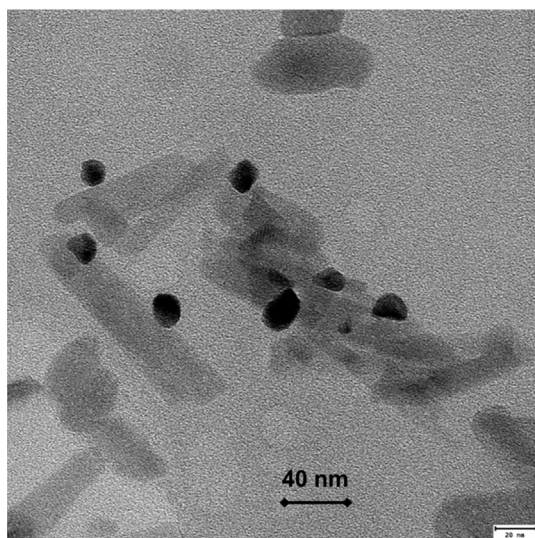
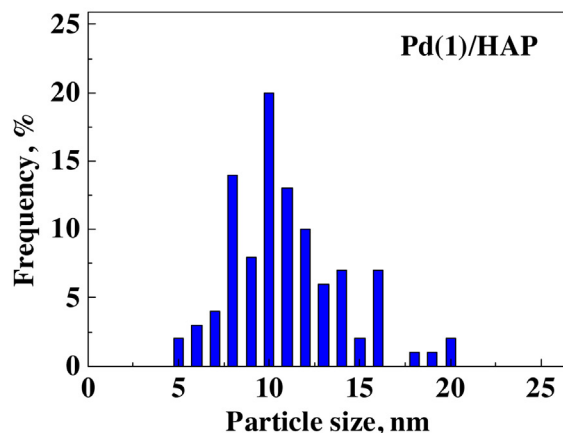
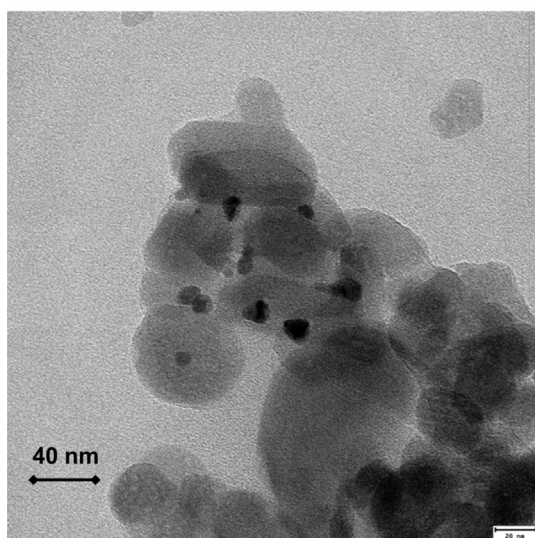
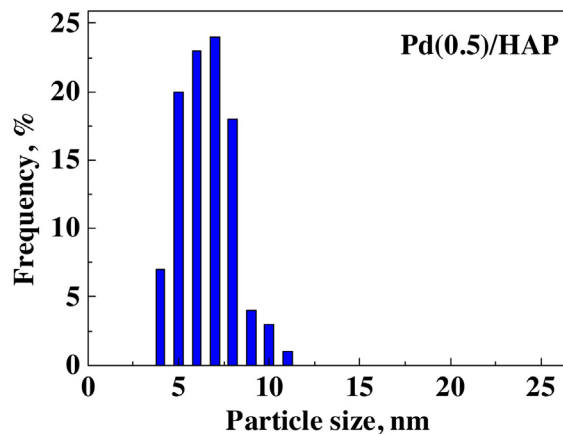
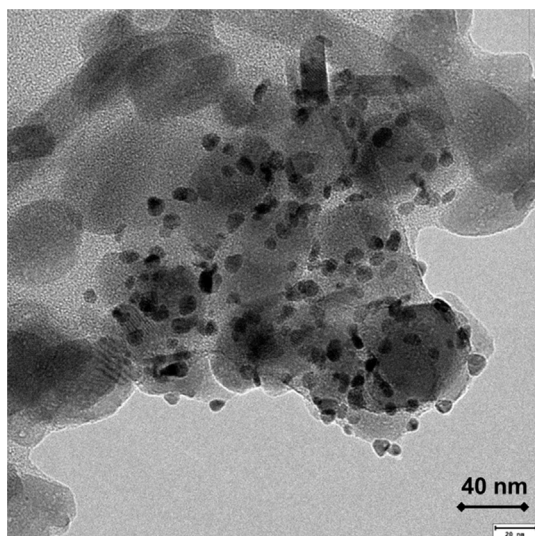


Fig. 2. TEM micrographs of the reduced Pd(x)/HAP catalysts.

HAP. For instance, the Pd(1)/HAP and Pd(2)/HAP samples exhibit a CO_2 production peak at 300 °C while the Pd(0.5)/HAP sample exhibits two peaks at 200 °C and 300 °C. Table 3 also lists the total

amounts of desorbed CO_2 extracted from the integration of its corresponding peaks. It can be observed that the addition of palladium onto the HAP surface dramatically increases the amount of the des-

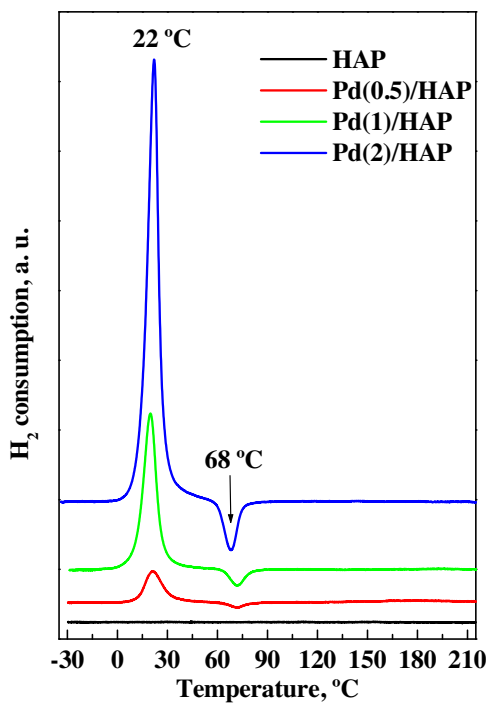


Fig. 3. H_2 -TPR profiles of the $\text{Pd}(x)/\text{HAP}$ catalysts.

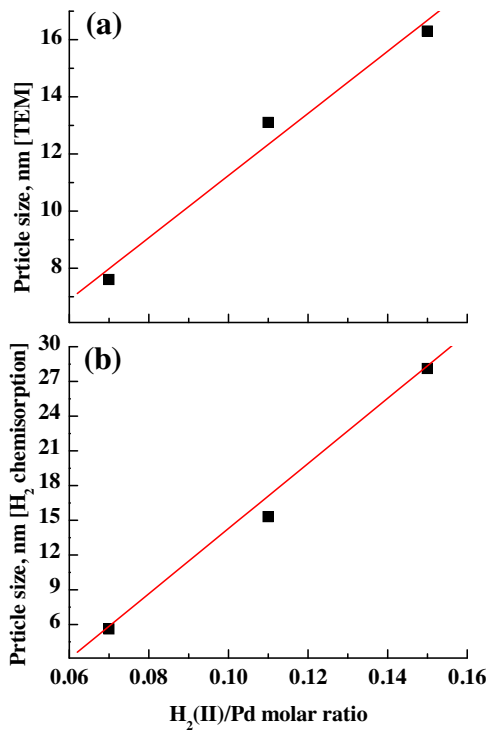


Fig. 4. Pd particle size, determined by (a) TEM and (b) H_2 chemisorption, dependence on the $\text{H}_2(\text{II})/\text{Pd}$ molar ratio (determined by H_2 -TPR).

orbed CO_2 . For instance, the surface density of CO_2 desorbed from the support, $0.8 \mu\text{mol g}_{\text{cat}}^{-1}$, is much smaller than that determined for $\text{Pd}(0.5)/\text{HAP}$, $4 \mu\text{mol g}_{\text{cat}}^{-1}$. The latter also demonstrates that it bears more active sites associated with the formation of CO_2 than the $\text{Pd}(1)/\text{HAP}$ and $\text{Pd}(2)/\text{HAP}$ catalysts ($2.7\text{--}2.9 \mu\text{mol g}^{-1}$). As suggested by the TPD traces for the three Pd catalysts (Fig. 5b) the loss observed in the density of these active sites observed upon

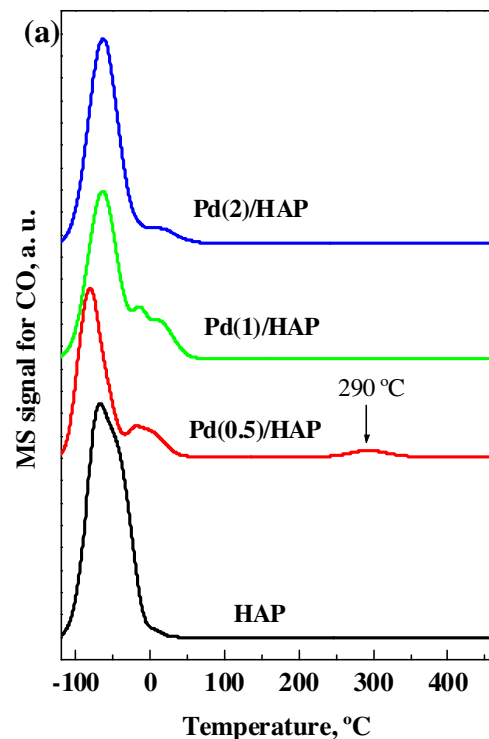


Fig. 5. TPD-MS study of CO pre-adsorbed on $\text{Pd}(x)/\text{HAP}$: spectra corresponding to the (a) $\text{m/z} = 28$ and (b) $\text{m/z} = 44$ signals.

increasing the palladium concentration may be correlated with the disappearance of the CO_2 desorption peak at 200°C , which can be associated with the presence of highly dispersed Pd species.

These remarkable differences between the $\text{Pd}(x)/\text{HAP}$ samples point out the effect of the Pd dispersion on the amount, distribution and activity of the CO adsorption sites. In this sense, the high dispersion of the Pd species decreases the density of the weak-

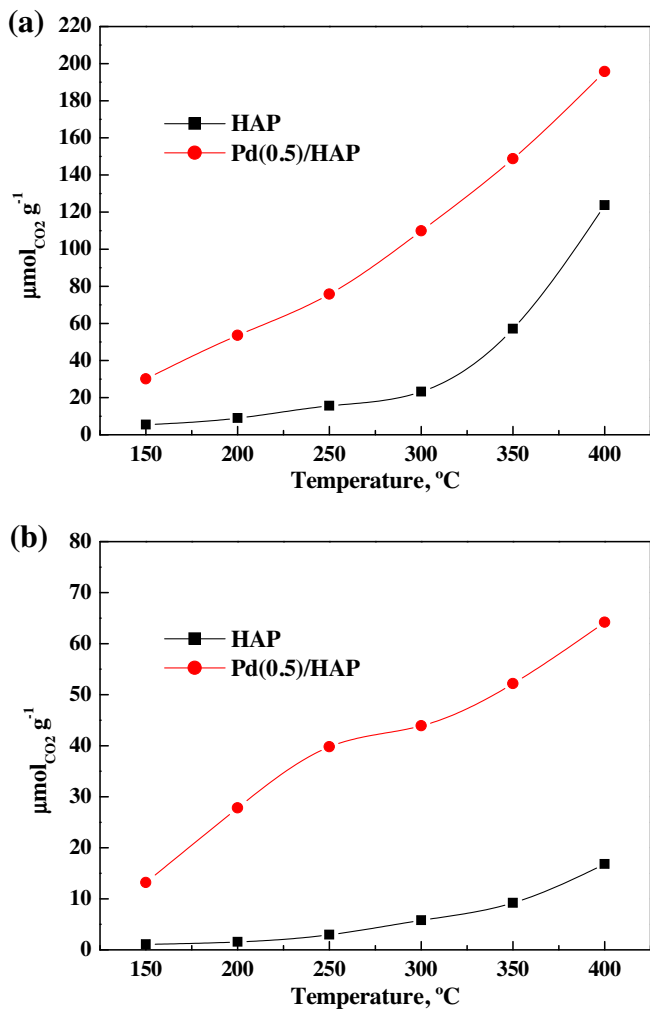


Fig. 6. Evolution of (a) OSCC and (b) OSC as a function of temperature over HAP bare support and Pd(0.5)/HAP catalyst.

strength adsorption sites of CO and increases the density of strong adsorption sites by providing extra active sites.

3.1.6. OSCC and OSC studies

The OSCC and OSC studies on the Pd(x)/HAP catalysts in the temperature range between 150°C and 400°C are summarized in Fig. 6 and Fig. 7. By means of OSCC valuable information about the maximum reducibility of the catalysts can be gained while the OSC results provide a quantification of the most reactive and available oxygen atoms.

As reported in Fig. 6a and b negligible amounts of CO₂ are released before 200°C on the HAP bare support. At higher temperatures, oxygen storage sites on the surface may be accessed. As temperature increases, the OSC and OSCC increases proceed via different pathways. OSC does not exceed 17 μmol CO₂ g⁻¹ at 400°C, Fig. 6b, probably because it is limited by the most reactive species located at the support surface. By contrast, much higher OSCC values are obtained in all the range of investigated temperatures (Fig. 6b). For instance it reaches 123 μmol CO₂ g⁻¹ at 400°C. This behavior, which represents the maximum reducibility, suggests that OSCC seems to be controlled by a participation of bulk oxygen. Nevertheless, all the OSCC and OSC values obtained on the HAP bare support, evidence its low activity compared to reducible supports. For instance, at 250°C the OSCC is around 15 μmol CO₂ g⁻¹ on HAP while much higher value, 550 μmol CO₂ g⁻¹, was obtained by Pastor-Pérez et al. [38] on ceria bare support. Likewise, HAP

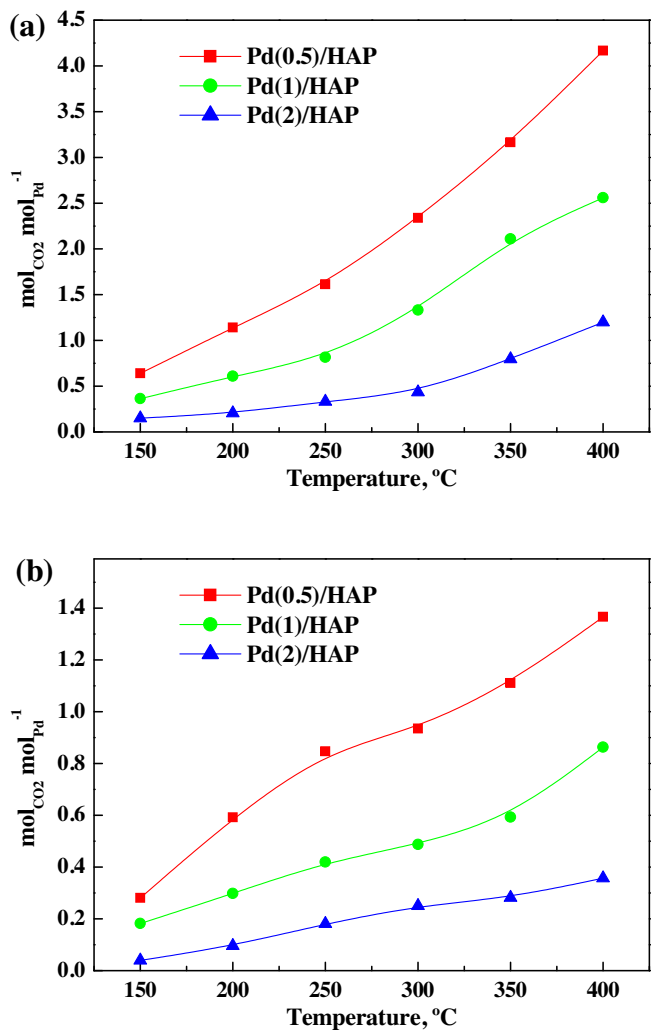


Fig. 7. Evolution of (a) OSCC and (b) OSC as a function of temperature over Pd(x)/HAP catalysts.

presents very low oxygen storage capacity, 2.9 μmol CO₂ g⁻¹, compared to ceria support (180 μmol CO₂ g⁻¹).

Irrespective of the Pd catalyst content, addition of palladium to the carrier generally increases both OSC and OSCC values of HAP (Fig. 6). For example, at 400°C, the OSC value obtained on the Pd(0.5)/HAP catalyst, 64.2 μmol CO₂ g⁻¹, is about four times higher than that exhibited by unsupported HAP (Fig. 6b). At the same temperature, it is observed that Pd addition improves the OSCC activity by only 1.6 times (Fig. 6a). This indicates that the effect of palladium on the oxygen storage capacity is more pronounced on the surface of HAP. Bedrane et al. [39] observed similar effect in their Pd/CZ catalysts and reported that metal particles can act as activators for the subsequent migration and storage of oxygen onto the support.

Fig. 7 compares the OSCC and OSC values, as a function of temperature, per total amount of palladium for the three Pd catalysts. The OSCC of the Pd(0.5)/HAP catalyst increases from 0.64 mol CO₂ mol_{Pd}⁻¹ at 150°C to 2.34 mol CO₂ mol_{Pd}⁻¹ at 300°C and 4.2 mol CO₂ mol_{Pd}⁻¹ at 400°C (Fig. 7a). These values are significantly higher than those corresponding to Pd(1)/HAP and Pd(2)/HAP catalysts; where the series of the catalysts follows this trend: Pd(0.5)/HAP > Pd(1)/HAP > Pd(2)/HAP. Fig. 7b reports the variation of CO₂ amounts, as a function of temperature, extracted from the OSC study. A comparison of the OSC values of the investigated Pd(x)/HAP catalysts shows that they keep the trend observed in the OSCC study. For instance, at 300°C, the OSC decreases from

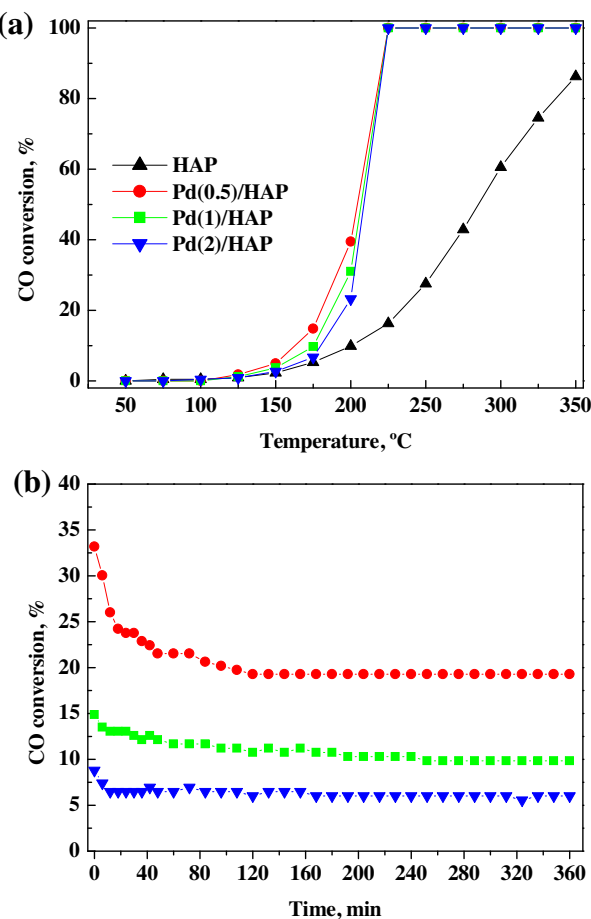


Fig. 8. CO oxidation over Pd(x)/HAP catalysts: (a) Light-off curves and (b) CO conversion at 175 °C as a function of time on stream.

0.94 mol_{CO2} mol_{Pd}⁻¹ for Pd(0.5)/HAP to 0.49 mol_{CO2} mol_{Pd}⁻¹ for Pd(1)/HAP and 0.25 mol_{CO2} mol_{Pd}⁻¹ for Pd(2)/HAP. These data suggest a notable improvement of the reducibility and the oxygen mobility of Pd species exhibiting relatively high dispersion on the HAP support. Similar conclusions were extracted by Reina et al. [40] which reported an improvement of oxygen mobility on supported metal providing higher surface/bulk ratios.

3.2. Catalytic activity

3.2.1. Activity in COTOX reaction

The catalytic activity of the prepared Pd(x)/HAP samples was investigated in the CO oxidation reaction. It should be noted that preliminary experiments (not shown), carried out on the oxidised and reduced Pd(x)/HAP samples, show that the latter exhibit the highest catalytic activity. This is consistent with earlier study from the literature which attributed the high performance of the pre-reduced Pd catalysts to an enhancement of the metal-support interaction, the formation of oxygen vacancies and enrichment in the surface hydroxyl groups [41].

Fig. 8a displays the CO conversion as a function of the COTOX reaction temperature over the reduced Pd(x)/HAP catalysts (light-off curves). With the reactor filled up with pure HAP the reaction starts around 150 °C to reach 50% of CO conversion at 280 °C; but it does not exceed 85% at 350 °C. Nevertheless, this behavior evidences the superiority of HAP activity when compared with alumina bare support [42]. The latter did not reach 15% conversion even for temperatures higher than 350 °C. Addition of palladium to the HAP carrier markedly improves its catalytic behavior (Fig. 8a).

Indeed, over the Pd(x)/HAP catalysts the activity begins around 110 °C and the CO conversion increases rapidly to reach 100% at about 225 °C. As reported in Table 4, the Pd loading does not affect significantly the temperature required for 50% (T₅₀) CO conversion (204–209 °C). The latter are slightly lower than that reported by Gaudet et al. [30] over their Pd/Al₂O₃ system where the corresponding T₅₀ value reached 212 °C. Likewise, our T₅₀ values are much lower than that of Pd/SiO₂ catalyst (275 °C), reported by Liu et al. [43]. A second catalytic run, performed on the same catalysts, shows a reproducibility of the obtained results. Table 4 also shows the turnover frequencies (TOF) values, normalised as the number of reacted CO molecules per surface Pd active sites determined by H₂ chemisorption and the values of the apparent activation energy determined in the temperature range of 125–175 °C. The TOF values calculated at 110 °C, 140 °C and 175 °C seem to decrease significantly with the Pd loading increase. For instance, at 140 °C the TOF decreases from 36.6 × 10⁻³ s⁻¹ for the Pd(0.5)/HAP catalyst to 21 × 10⁻³ s⁻¹ for Pd(2)/HAP. Likewise, at 175 °C, the Pd(0.5)/HAP (133.8 × 10⁻³ s⁻¹) results two time more active than the Pd(2)/HAP catalyst (67.2 × 10⁻³ s⁻¹). Taking into account the similar active Pd surface area measured on the three catalysts (0.42–0.47 m² Pd g⁻¹) this tendency suggests that the Pd particle size plays a key role in the activity of the investigated Pd(x)/HAP catalysts in COTOX reaction. In agreement with our TEM and H₂ chemisorptions studies highly dispersed Pd species exhibiting the smallest Pd particles size are detected on the Pd(0.5)/HAP catalyst. This finding points out that over Pd(x)/HAP catalysts the CO oxidation is a structure-sensitive catalytic reaction. It should be noted that the structure-sensitivity of CO oxidation on the Pd catalysts is a subject of controversy. For instance, in agreement with our activity results, Jin et al. [44] reported that the catalytic activity of their Pd/ZnO catalysts in CO oxidation was significantly enhanced when the size of Pd nanocrystals was reduced from 18 nm to 6 nm. By contrast, in their study on the effect of Pd dispersion on the catalytic activity of Pd/Al₂O₃ systems in CO oxidation, Haneda et al. [14] claimed that the CO oxidation over Pd/Al₂O₃ is a structure-insensitive reaction.

A comparison of our results with those reported in previous study [30] shows that lower TOF values were obtained over Pd/Al₂O₃ systems which did not exceed 1.92 × 10⁻³ s⁻¹ at 110 °C (versus 5.4–7.1 × 10⁻³ s⁻¹ over Pd(x)/HAP catalysts). This comparison proves that the HAP appears as a good alternative to the alumina support. Table 1 also lists the textural properties of the assayed catalysts in the COTOX reaction. The results show that no significant changes are observed in their specific surface areas and in their mean pore size after two reaction cycles. Similar results were reported by Shen et al. [45] in their study on the activity of Pd catalysts supported on phosphorous modified alumina support. They found that the interaction between Pd clusters and P-O-Al units in the P-doped Al₂O₃ prevents the sintering of Pd and the phase segregation of AlPO₄ in γ-Al₂O₃.

On the other hand, the apparent activation energies values, obtained from Arrhenius plots, are almost similar (59–60 kJ mol⁻¹) suggesting that irrespective of the used Pd catalyst the CO oxidation reaction occurs through the same mechanism (Table 4). Note that the obtained values are in good agreement with a number of earlier studies dealing with the oxidation of CO over Pd catalysts [30,46].

In order to examine the stability of the prepared Pd(x)/HAP samples catalytic runs were conducted at 175 °C for a considerably prolonged reaction time interval (6 h) (Fig. 8b). As expected, the Pd(0.5)/HAP sample exhibits the highest initial conversion value (33%) compared to 15% for Pd(1)/HAP and 9% for Pd(2)/HAP. However, CO conversion over the former rapidly decreases during the first 2 h after which it tends to reach a stationary state corresponding to a conversion of 19%. By contrast, over the Pd(1)/HAP and

Table 4

Activity data of Pd(x)/HAP catalysts in the COTOX reaction.

Catalysts	T ₅₀ , °C	TOF ₁₁₀ (× 10 ³ s ⁻¹)	TOF ₁₄₀ (× 10 ³ s ⁻¹)	TOF ₁₇₅ (× 10 ³ s ⁻¹)	E _a , kJ mol ⁻¹ (125–175 °C)
Pd(0.5)/HAP	204	7.1	36.6	133.8	62.3
Pd(1)/HAP	207	5.4	31.1	113.0	61.9
Pd(2)/HAP	209	6.5	21.0	67.2	59.8

Pd(2)/HAP catalysts lower rates of deactivation are observed. The difference in the deactivation rate between the catalysts can be attributed to the capacity of each one to strongly adsorb CO. Our CO-TPD study, discussed above, highlights the presence of extra sites, which adsorb strongly the CO molecules, on the Pd(0.5)/HAP catalyst surface. This may explain the high rate of deactivation observed on this catalyst due to the blockage of the active sites by CO.

Given the promising behavior of Pd(0.5)/HAP catalyst additional experiments were performed to obtain a simple power law that describes the kinetics of the CO oxidation. The reaction rates were determined at 160 °C for low CO conversions, which corresponds to differential reactor conditions, and ensuring stable activity of the catalyst. Fig. S2(a) and Fig. S2(b) (supporting information) show the effect of CO and O₂ partial pressures, respectively, on the CO oxidation reaction rate. The latter seems to increase monotonically with O₂ partial pressure while it decreases with CO partial pressure; so a negative order with respect to CO is expected. Furthermore, logarithmic plot showing the dependence of the reaction rate on the CO and O₂ partial pressures are displayed in Fig. 9a and b, respectively. The analysis of the obtained results shows that the reaction order of CO and O₂ are -0.30 and 0.46, respectively. These kinetic data are consistent with those reported by Satsuma et al. [47] over Pd/Al₂O₃, Pd/ZrO₂ and Pd/SiO₂ catalysts. So, they proposed Langmuir-Hinselwood mechanism involving a dissociation of oxygen molecule on the metal surface. They attributed, moreover, the negative order respect to CO to self-poisoning of Pd surface by strongly adsorbed CO at low temperatures.

3.2.2. Activity in COPROX

Fig. 10a and b show the curves corresponding to the CO conversion and the selectivity to the CO₂ formation, in the COPROX reaction, over the Pd(x)/HAP catalysts. Note that carbon dioxide is the unique carbonaceous product detected (no formation of CH₄ is observed). Table 5 lists the temperatures corresponding to a conversion of 10%, the TOF determined at 175 °C and the activation energy values in the temperature range 100–175 °C.

As shown in Fig. 10 two temperature regions could be discussed in the activity profiles: at low temperatures (≤ 275 °C) X_{CO} increases with temperature to achieve 24% at 275 °C and a selectivity around 12%. When compared to their activity in the COTOX reaction the activity in the COPROX appears to be strongly influenced by the presence of H₂ in the gas mixture. For instance, at 100 °C, under the COPROX reactants gas mixture, X_{CO} reaches 6% on the Pd(0.5)/HAP catalyst while it is negligible in the COTOX reaction. Therefore, the enhanced low temperature reaction activity (75 °C $\leq T < 150$ °C) could be attributed to the presence of H₂ which promotes the initiation of the CO oxidation. This promotional effect of H₂ on CO oxidation was reported in several studies dealing with the activity of noble metals catalysts in the COPROX reaction [48–50].

By contrast, at high temperatures both X_{CO} and S_{CO₂} decrease with the reaction temperature suggesting the main occurrence of the H₂ oxidation at the expense of the CO oxidation. These results are in good agreement with earlier studies dealing with the activity of Pd supported catalysts in COPROX [51,52]. They explained the low activity at higher temperature to the presence of hydrogen which is preferentially adsorbed and easily oxidised, rather than CO, on metallic Pd. Moreover, as reported in Table 1, the characterization of Pd(x)/HAP post-reaction catalysts by N₂ physisorption

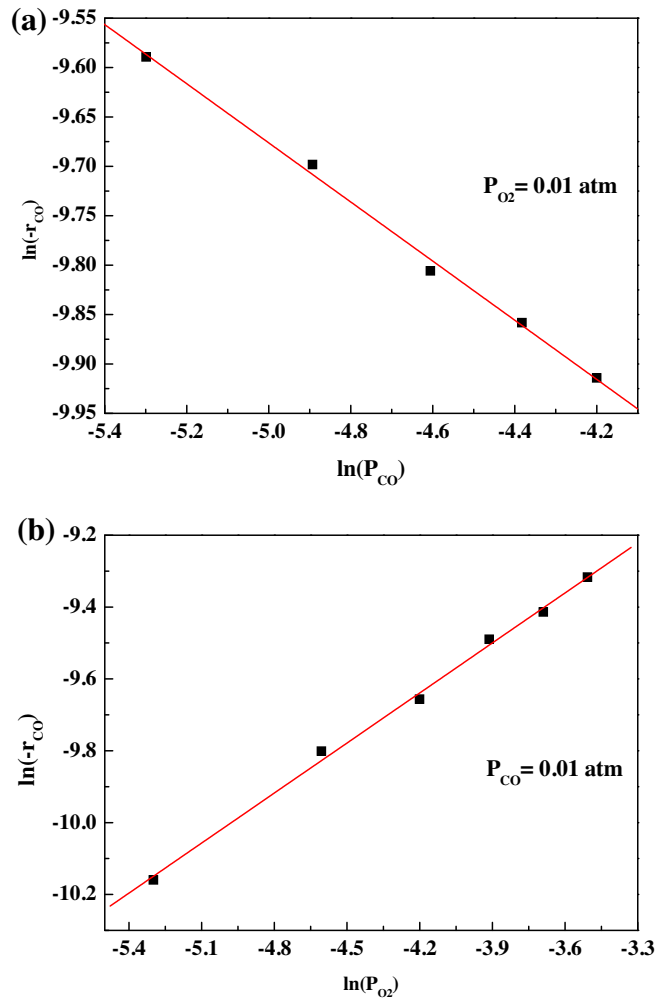


Fig. 9. Logarithmic plot of reaction rate at 160 °C vs partial pressure of (a) CO and (b) O₂ over Pd(0.5)/HAP catalyst.

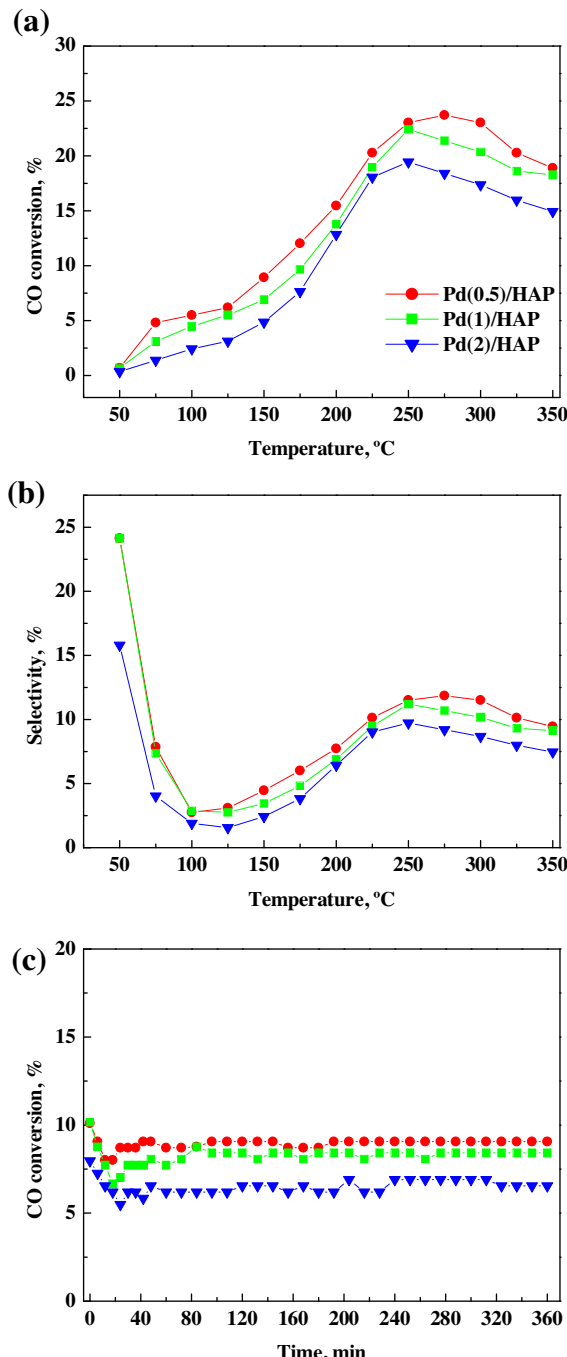
techniques shows an apparent drop in their specific surface areas (about 31–35%). These results were, however, expected in the presence of very high concentration of H₂ (60%) and water vapor as a product of its oxidation [54]. Nevertheless, CO conversion over the Pd(x)/HAP catalysts exceeds significantly that obtained over 1% Pd/CeO₂ catalyst used in the same O₂ excess conditions ($\lambda = 2$). The CO conversion on the latter, previously reported by Pozdnyakova et al. [51], did not reach 12% even at 300 °C (versus 17–24% reached over our Pd(x)/HAP catalysts). The performance of our Pd supported catalysts is also compared with that of 1%Pd/Ce_{0.63}Zr_{0.37}O₂ catalysts reported by Mariño et al. [53]. The latter obtained lower values in terms of CO conversions (<10%) and selectivity (<15%) in all the investigated temperature range (50–250 °C). This comparison shows a clear catalytic performance superiority of our Pd(x)/HAP catalysts.

The TOF values determined at 175 °C are included in Table 5. Over the Pd(0.5)/HAP and Pd(1)/HAP catalysts the TOF are about 110×10^{-3} s⁻¹ whereas the lowest value (84×10^{-3} s⁻¹) is obtained

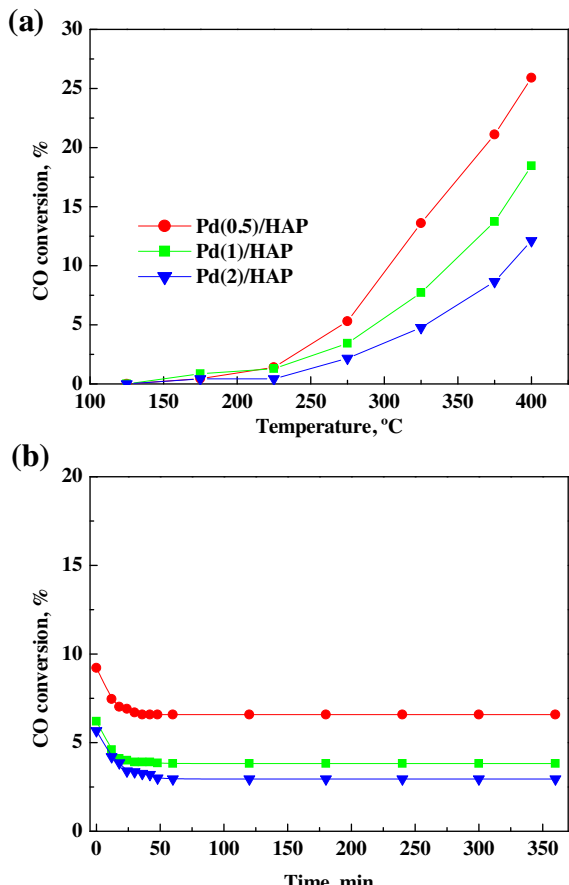
Table 5

Activity data of Pd(x)/HAP catalysts in the COPROX and WGS reactions.

Catalysts	COPROX			WGS		
	T ₁₀ , °C	TOF ₁₇₅ (× 10 ³ s ⁻¹)	E _a , kJ mol ⁻¹ (125–175 °C)	T ₁₀ , °C	TOF ₂₇₅ (× 10 ³ s ⁻¹)	E _a , kJ mol ⁻¹ (225–325 °C)
Pd(0.5)/HAP	160	110	19.7	300	47.3	56.3
Pd(1)/HAP	177	112	16.5	345	40.0	44.3
Pd(2)/HAP	187	84	26.4	385	21.8	59.7

**Fig. 10.** Activity of the Pd(x)/HAP catalysts in COPROX: (a) CO conversion, (b) selectivity to CO₂ and (c) CO conversion at 175 °C as a function of time on stream.

on the Pd(2)/HAP catalyst. The difference between the Pd(x)/HAP catalysts is probably related to the distribution of the active palladium species. The superior activity of the Pd(0.5)/HAP and Pd(1)/HAP samples suggests that they possess more efficient palla-

**Fig. 11.** WGS reaction over Pd(x)/HAP catalysts: (a) Light-off curves and (b) CO conversion at 275 °C as a function of time on stream.

dium sites than those deposited on Pd(2)/HAP catalyst. According to the TEM and H₂ chemisorption results on the latter larger Pd particles are deposited which also makes it less active and stable, at 175 °C, during 6 h on stream (Fig. 10c). The activation energy values on the Pd(x)/HAP catalysts are also listed in Table 5. These values, 16.5–26.4 kJ mol⁻¹, are considered very low when compared to those obtained in the COTOX reaction (about 60 kJ mol⁻¹). Hence, this overall activation energy barrier lowering is consistent with the above-mentioned proposal which points out the promotional effect of H₂ on the CO oxidation reaction.

3.2.3. Activity in WGS reaction

The performance and the stability of the Pd(x)/HAP catalysts were also studied in the WGS reaction. The catalysts were submitted to the same pre-treatment routine realized before the COTOX and the COPROX experiments (reduction at 200 °C). Fig. 11a and b show the light-off curves and the CO conversion as function of time on stream (at 275 °C), respectively.

On all the assayed Pd(x)/HAP samples CO activation starts around 150 °C after which, depending on the Pd loading, the conversion increases with the reaction temperature via different

pathways (Fig. 11a). For instance, the Pd(0.5)/HAP catalyst exhibits the lowest temperature required to reach a conversion of 10% (300 °C) whereas higher temperatures are needed in the case of Pd(1)/HAP and Pd(2)/HAP catalysts (345 °C and 385 °C, respectively). Likewise, the catalyst with the highest palladium loading (2%) exhibits the poorest performance at 400 °C with a conversion lower than 12%. This may be associated to the low dispersion of Pd and, then, the low density of the metal-support interface sites required for the WGS reaction [22]. However, the Pd(0.5)/HAP sample proves the best catalytic performance at 400 °C with a conversion reaching 26%. As discussed above, it is probably the metal-support interaction features that make of the hydroxyapatite such interesting carrier. For instance, in their study on the WGS reaction over Pd/Al₂O₃ catalysts, Lupescu et al. [22] found a conversion below 11% at 400 °C. They attributed the poor activity of their catalysts to the lack of oxygen mobility in the support material. On another hand, the Pd(x)/HAP catalysts demonstrate good resistance against surface area loss (Table 1).

Fig. 11b displays the activity of the Pd(x)/HAP as a function of time on stream at 275 °C. A comparison of the initial conversion shows that the Pd(0.5)/HAP sample presents the highest value (9%) compared to 5% for Pd(1)/HAP and 6% for Pd(2)/HAP. However, on all the assayed catalysts, CO conversion presents an apparent instability during the first 1 h. After this instability period the activity stays almost constant corresponding to a conversion of 7% for Pd(0.5)/HAP, 4% for Pd(1)/HAP and 3% for Pd(2)/HAP catalyst.

Table 5 also lists the specific catalytic activity (TOF, at 275 °C) and the activation energy values for the three Pd(x)/HAP catalysts. A comparison of the apparent E_a for the assayed samples, 44.3–59.7 kJ mol⁻¹, to those reported in the literature shows that they are quite similar [22]. The TOF values seem to follow similar tendency compared to that observed in COTOX and COPROX reactions. Indeed, TOF decreases from 47 × 10⁻³ s⁻¹ over Pd(0.5)/HAP to 22 × 10⁻³ s⁻¹ for Pd(2)/HAP. It is admitted that the activity in WGS reaction is related to the reducibility and the oxygen storage capacity of the catalyst [22]. In this sense, the high performance of our Pd(0.5)/HAP catalyst could be explained by the presence of small Pd particle sizes that present higher reducibility and higher oxygen storage capacity.

4. Conclusion

Pd(x)/hydroxyapatite catalysts (0.5 ≤ x ≤ 2) have been synthesised and characterised by a wide number of analytical techniques including N₂ physisorption, XRD, H₂-TPR, H₂ chemisorption, TEM, CO-TPD, OSCC and OSC techniques. The characterisation results show the presence of a fraction representing 0.3 wt.% Pd which has been incorporated into the hydroxyapatite network and the deposition of Pd species spread as metallic Pd over the carrier. The chemical and physical properties of the latter are affected by the Pd content. Due to its smaller Pd particle sizes the Pd(0.5)/HAP catalyst demonstrates stronger CO adsorption, higher reducibility in the presence of CO and higher oxygen mobility compared to the high loading samples (1% and 2%). These interesting features seem to contribute in the enhancement of the activity and selectivity in the three investigated CO elimination processes (COTOX, COPROX and WGS). By contrast, despite exhibiting similar active Pd surface area, compared to those measured on Pd(0.5)/HAP and Pd(1)/HAP, the Pd-rich catalyst (2%) exhibits the poorest performance. This finding points out that over Pd(x)/HAP catalysts the CO oxidation via the three processes is a structure-sensitive catalytic reaction where the distribution of the Pd species plays a key role in their performance. Moreover, the performances of the Pd/HAP catalysts evidence the potential of HAP support as promising alternative to those reported in the available literature.

Work is in progress toward improving the activity and selectivity of Pd(x)/HAP catalysts through the use of promoters.

Acknowledgements

The financial support for this work provided by Gobierno Vasco (GIC IT-657-13) and Ministerio de Economía y Competitividad (ENE2013-41187-R) is gratefully acknowledged. Likewise, the technical support provided by SGIker (UPV/EHU) is gratefully acknowledged.

Appendix A. Supplementary data

Supplementary data associated with this article can be found, in the online version, at <http://dx.doi.org/10.1016/j.apcatb.2016.08.039>.

References

- [1] K. Liu, A. Wang, T. Zhang, *ACS Catal.* 2 (2012) 1165–1178.
- [2] Z. Boukha, J.L. Ayastuy, A. Iglesias-González, B. Pereda-Ayo, M.A. Gutiérrez-Ortiz, J.R. González-Velasco, *Int. J. Hydrogen Energy* 40 (2015) 7318–7328.
- [3] Z. Boukha, J.L. Ayastuy, A. Iglesias-González, B. Pereda-Ayo, M.A. Gutiérrez-Ortiz, J.R. González-Velasco, *Appl. Catal. B* 160–161 (2014) 629–640.
- [4] N.K. Gamboa-Rosales, J.L. Ayastuy, Z. Boukha, N. Bion, D. Duprez, J.A. Pérez-Omil, E. del Río, M.A. Gutiérrez-Ortiz, *Appl. Catal. B* 168–169 (2015) 87–97.
- [5] Y. Zhou, Z. Wang, C. Liu, *Catal. Sci. Technol.* 5 (2015) 69–81.
- [6] A. Satsuma, K. Osaki, M. Yanagihara, J. Ohyama, K. Shimizu, *Appl. Catal. B* 132–133 (2013) 511–518.
- [7] H. Zhu, Z. Qin, W. Shan, W. Shen, J. Wang, *J. Catal.* 225 (2004) 267–277.
- [8] L. Liu, F. Zhou, L. Wang, X. Qi, F. Shi, Y. Deng, *J. Catal.* 274 (2010) 1–10.
- [9] D.I. Kochubey, S.N. Pavlova, B.N. Novgorodov, G.N. Kryukova, V.A. Sadykov, *J. Catal.* 161 (1996) 500–506.
- [10] Y. Li, Y. Yu, J.- Wang, J. Song, Q. Li, M. Dong, C.- Liu, *Appl. Catal. B* 125 (2012) 189–196.
- [11] K. Tanikawa, C. Egawa, *Appl. Catal. A* 403 (2011) 12–17.
- [12] R.S. Johnson, A. DeLaRiva, V. Ashbacher, B. Halevi, C.J. Villanueva, G.K. Smith, S. Lin, A.K. Datye, H. Guo, *Phys. Chem. Chem. Phys.* 15 (2013) 7768–7776.
- [13] Y. Zhou, Z. Wang, C. Liu, *Catal. Sci. Technol.* 5 (2015) 69–81.
- [14] M. Haneda, M. Todo, Y. Nakamura, M. Hattori, *Catal. Today* (2016), <http://dx.doi.org/10.1016/j.cattod.2016.05.025>.
- [15] S.H. Oh, R.M. Sinkevitch, *J. Catal.* 142 (1993) 254.
- [16] O. Pozdnyakova, D. Teschner, A. Wootsch, J. Kröhnert, B. Steinhauer, H. Sauer, L. Toth, F.C. Jentoft, A. Knop-Gericke, Z. Paál, R. Schlögl, *J. Catal.* 237 (2006) 17–28.
- [17] F. Marino, C. Desorme, D. Duprez, *Appl. Catal. B* 54 (2004) 59–66.
- [18] Y. Sekine, T. Chihara, R. Watanabe, Y. Sakamoto, M. Matsukata, E. Kikuchi, *Catal. Lett.* 140 (2010) 184–188.
- [19] Y. Sekine, H. Takamatsu, S. Aramaki, K. Ichishima, M. Takada, M. Matsukata, E. Kikuchi, *Appl. Catal. A* 352 (2009) 214–222.
- [20] S. Hilaire, X. Wang, T. Luo, R.J. Gorte, J. Wagner, *Appl. Catal. A* 215 (2001) 271–278.
- [21] T. Bunluesin, R.J. Gorte, G.W. Graham, *Appl. Catal. B* 15 (1998) 107–114.
- [22] J.A. Lupescu, J.W. Schwank, K.A. Dahlberg, C.Y. Seo, G.B. Fisher, S.L. Peczonczyk, K. Rhodes, M.J. Jagner, L.P. Haack, *Appl. Catal. B* 183 (2016) 343–360.
- [23] J.A. Lupescu, J.W. Schwank, G.B. Fisher, X. Chen, S.L. Peczonczyk, A.R. Drews, *Appl. Catal. B* 185 (2016) 189–202.
- [24] Z. Boukha, J. González-Prior, B.d. Rivas, J.R. González-Velasco, R. López-Fonseca, J.I. Gutiérrez-Ortiz, *Appl. Catal. B* 190 (2016) 125–136.
- [25] Z. Boukha, M. Kacimi, M.F.R. Pereira, J.L. Faria, J.L. Figueiredo, M. Ziyad, *Appl. Catal. A* 317 (2007) 299–309.
- [26] Z. Boukha, M. Kacimi, M. Ziyad, A. Ensuque, F. Bozon-Verduraz, *J. Mol. Catal. A* 270 (2007) 205–213.
- [27] A. Borodzinski, M. Bonarowska, *Langmuir* 13 (1997) 5613–5620.
- [28] M.A. Aramendia, V. Borau, C. Jimenez, J.M. Marinas, A. Moreno, *Colloid Surf. A* 106 (1996) 161–165.
- [29] J.L. Ayastuy, A. Gurbani, M.P. González-Marcos, M.A. Gutiérrez-Ortiz, *Ind. Eng. Chem. Res.* 48 (2009) 5633–5641.
- [30] J.R. Gaudet, A. de la Riva, E.J. Peterson, T. Bolin, A.K. Datye, *ACS Catal.* 3 (5) (2013) 846–855.
- [31] J. Panpranot, O. Tangjittwattakorn, P. Praserthdam, J.G. Goodwin, *Appl. Catal. A* 292 (2005) 322–327.
- [32] W.J. Shen, M. Okumura, Y. Matsumura, M. Haruta, *Appl. Catal. A* 213 (2001) 225–232.
- [33] G. Neri, M.G. Musolino, C. Milone, D. Pietropaolo, S. Glavagno, *Appl. Catal. A* 208 (2001) 307–316.
- [34] J. Wang, H. Chen, Z. Hu, M. Yao, Y. Li, *Catal. Rev. Sci. Eng.* 57 (2015) 79–144.

[35] F.B. Noronha, M.A.S. Baldanza, M. Schmal, *J. Catal.* 188 (1999) 270–280.

[36] J.S. Rieck, A.T. Bell, *J. Catal.* 96 (1985) 88–105.

[37] J.S. Rieck, A.T. Bell, *J. Catal.* 103 (1987) 46–54.

[38] L. Pastor-Pérez, T.R. Reina, S. Ivanova, M.A. Centeno, J.A. Odriozola, A. Sepúlveda-Escribano, *Catalysts* 5 (2015) 298–309.

[39] S. Bedrane, C. Descorme, D. Duprez, *Catal. Today* 73 (2002) 233–238.

[40] T.R. Reina, S. Ivanova, J.J. Delgado, I. Ivanov, V. Idakiev, T. Tabakova, M.A. Centeno, J.A. Odriozola, *ChemCatChem* 6 (2014) 1401–1409.

[41] M. Jin, J. Park, J.K. Shon, J.H. Kim, Z. Li, Y. Park, J.M. Kim, *Catal. Today* 185 (2012) 183–190.

[42] T.R. Reina, S. Ivanova, M.A. Centeno, J.A. Odriozola, *Front. Chem.* 12 (2013) 1–9.

[43] X. Liu, R. Wang, L. Song, H. He, G. Zhang, X. Zi, W. Qiu, *Catal. Commun.* 46 (2014) 213–218.

[44] M. Jin, H. Liu, H. Zhang, Z. Xie, J. Liu, Y. Xia, *Nano. Res.* 4 (2011) 83–91.

[45] M. Shen, L. Song, J. Wang, X. Wang, *Catal. Commun.* 22 (2012) 28–33.

[46] Y. Li, Y. Yu, J. Wang, J. Song, Q. Li, M. Dong, C. Liu, *Appl. Catal. B* 125 (2012) 189–196.

[47] A. Satsuma, K. Osaki, M. Yanagihara, J. Ohyama, K. Shimizu, *Appl. Catal. B* 132–133 (2013) 511–518.

[48] T. Nguyen, F. Morfin, M. Aouine, F. Bosselet, J. Rousset, L. Piccolo, *Catal. Today* 253 (2015) 106–114.

[49] S. Salomons, R.E. Hayes, M. Votsmeier, *Appl. Catal. A* 352 (2009) 27–34.

[50] M.J. Kahlich, H.A. Gasteiger, R.J. Behm, *J. Catal.* 171 (1997) 93–105.

[51] O. Pozdnyakova, D. Teschner, A. Wootsch, J. Kröhnert, B. Steinhauer, H. Sauer, L. Toth, F.C. Jentoft, A. Knop-Gericke, Z. Paál, R. Schlögl, *J. Catal.* 237 (2006) 17–28.

[52] M. Navlani-García, I. Miguel-García, A. Berenguer-Murcia, D. Lozano-Castelló, D. Cazorla-Amorós, H. Yamashita, *Catal. Sci. Technol.* 6 (2016) 2623.

[53] F. Mariño, C. Descorme, D. Duprez, *Appl. Catal. B* 54 (2004) 59.

[54] C.H. Bartholomew, *Appl. Catal. A* 212 (2001) 17–60.